Online ISSN: 2981-0396 Print ISSN: 2981-0388

International Journal of Iron & Steel Society of Iran

Journal Homepage: https://journal.issiran.com/

Research Note

Effect of laser power on microstructure and tensile properties of laser welded DP590 steel joints

H. Ashrafi *[1], A. R. Shahsavari [2], A. Ghandi [3]

[1,2] *Faculty of Chemical and Materials Engineering, Shahrood University of Technology, Shahrood, Iran*
[3] *Department of Materials Engineering, Isfahan University of Technology, Isfahan, Iran*

ARTICLE INFO

Keywords:

Dual phase steel, laser welding, laser power, Microstructure, Tensile properties.

Article history:

Received 05 August 2023
Received in revised from 04 October 2023
Accepted 09 March 2024

ABSTRACT

This study investigated the effects of varying laser power on the microstructure and tensile properties of DP590 steel joints. Three joints were prepared using three different laser power levels (400W, 450W, and 500W), while keeping all other factors constant. The results indicated that laser welding resulted in the formation of martensite in the fusion zone, leading to a notable increase in hardness. However, with increasing the laser power, the hardness increment decreased due to the presence of acicular ferrite and Widmanstatten ferrite alongside martensite. The heat-affected zone (HAZ) of all welds exhibited a region where hardness dropped below that of the base metal (BM) due to partial tempering of martensite. This softening effect intensified with higher laser power. The sample welded with a laser power of 400W failed early in the tensile test due to lack of penetration. Conversely, the other two samples failed within the softened zone, showing yield strength values similar to the BM and high joint efficiency values (92.5% for 450W and 89.5% for 500W) but with a noticeable reduction in elongation. Both DP590 steel and welded joints exhibited a two-stage work hardening behavior consisting of a transient stage followed by a stage III hardening.

1. Introduction

Advanced high strength steels (AHSS) have gained significant attention in recent decades, particularly in the automotive sector [1]. These steels provide several benefits such as enhanced tensile strength and work hardening rates. This enables the production of components that are simultaneously lighter and stronger. Consequently, there is a noticeable improvement in performance, fuel efficiency, safety measures, and various other advantages [2, 3].

One of the frequently utilized types of AHSS in the car manufacturing sector is known as dual phase (DP) steel, which consists of a ferritic structure with varying amount of martensite islands, depending on the steel grade [4]. The combination of ferrite ductility and martensite strength in DP steels results in exceptional mechanical properties, making them ideal for parts undergoing forming processes. These properties include high ultimate tensile strength (UTS), a high work hardening rate, and a low yield strength (YS) to UTS ratio [5].

The use of DP steel sheets in industrial applications typically involves the use of joining processes, either before or after its shaping. Among these processes, one of the most commonly used is laser welding (LW), which offers

**Corresponding author*
Email: hashrafi@shahroodut.ac.ir
Address: Faculty of Chemical and Materials Engineering, Shahrood University of Technology, Shahrood 3619995161, Iran
1. Assistant Professor, 2. Bsc, 3. PhD.

http://doi.org/10.22034/IJISSI.2024.2008540.1269
Published by ISSI (Iron & Steel Society of Iran)

excellent mechanical properties in the joined area and can be easily automated, making it highly flexible for various applications [6]. Numerous studies have been conducted on the LW of DP steels. For instance, Farabi et al. [7] examined the microstructure and mechanical properties of laser welded dissimilar DP600/DP980 joints. They noted a significant increase in hardness in the fusion zone (FZ) and the formation of a softened zone in the heat-affected zone (HAZ). Xia et al. [8] utilized the normalized Rosenthals equation and Vickers hardness testing to investigate how the heat input and martensite volume fraction affect the softening behavior of the HAZ in laser welded DP steels. Their research revealed a direct relationship between the extent of HAZ softening and the martensite volume fraction resulting from martensite tempering. Mostaan et al. [9] examined the impact of silicon content on the microstructure and mechanical properties of laser welded DP steels. They found that the UTS of welded samples increased with an increase in silicon content.

The above literature review showed that the mechanical characteristics of laser welded DP steel joints are influenced by factors such as the steel's chemical composition, the proportion of martensite, and the heat input during welding. This study focused on examining how the microstructure and tensile properties of diode laser beam welded DP590 steel joints are affected by the laser power.

2. Materials and methods

The as-received DP590 steel sheet (POSCO, South Korea) with a thickness of 1.6 mm was used in this study. The chemical composition of the steel is listed in Table 1.

LW was conducted with a diode laser machine, employing the parameters indicated in Table 2. A shielding gas of argon, with a flow rate of 10L/min, was used. Two DP590 steel sheets of identical dimensions (40 mm × 100 mm) were joined together in a butt joint configuration. Metallographic samples were extracted from the weld cross-section, as schematically shown in Fig. 1a, and observed under an optical microscope after being ground to a 2500 grit finish, polished using a 0.3 μm alumina suspension, and etched with a 3% Nital solution. The volume fraction of martensite in the BM was determined by analyzing optical microscopy (OM) images using the image J software. Microhardness tests were conducted using a Vickers microhardness tester (Buehler, Germany) with a load of 100g and a holding time of 10s. The indentation points were spaced adequately to prevent any potential influence from strain fields caused by adjacent indentations.

In order to determine the tensile properties, uniaxial tensile tests were conducted on both the BM and welded joints, using a Hounsfield H50KS machine, with a crosshead speed of 1 mm/min. The location of the tensile tests specimens is schematically illustrated in Fig. 1a. Tensile specimens were prepared from the BM and welded samples using electrical discharge machining, with the dimensions shown in Fig. 1b. Two specimens were tested for each condition, and the average values of the tensile properties were reported.

Table 1. Chemical composition (wt.%) of DP590 steel used in this research.

Fe	C	Si	Mn	P	S	Cr	Mo	Ni	V	Ti	Cu	Al
Bal.	0.073	0.321	1.871	0.024	0.005	0.012	max 0.005	max 0.005	max 0.002	0.006	0.038	0.039

Table 2. Processing parameters of LW operations.

sample	Welding speed (mm/min)	Laser power (W)
LW400	50	400
LW450	50	450
LW500	50	500

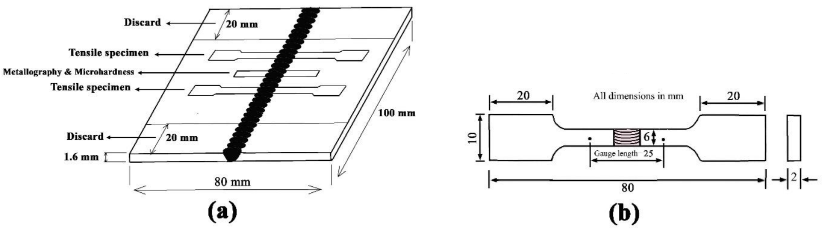

Fig. 1. Geometry and dimensions of the tensile specimens.

3. Results and discussion

3.1. Macrostructure and microstructure

Fig. 2. provides an overview of the cross-sectional view of welds in DP590 steel. The cross-section of the welds displays a heterogeneous structure across different areas of the joint, such as the FZ, coarse-grained HAZ (CGHAZ), fine-grained HAZ (FGHAZ), subcritical HAZ (SCHAZ), and BM. The LW400 sample showed a lack of penetration defect (marked by arrow in Fig. 2a.), whereas the other two samples displayed complete penetration. Additionally, it was observed that increasing the LW power resulted in the widening of the FZ and HAZ.

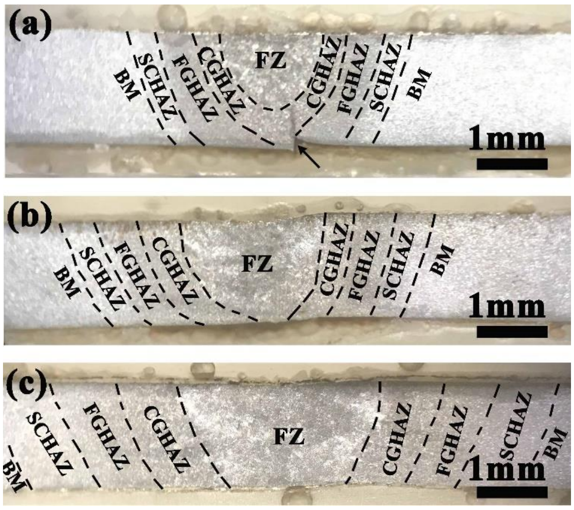

Fig. 2. Macroscopic image of the welded samples: (a) LW400, (b) LW450, (c) LW500.

Fig. 3. shows the OM image of the microstructure of the DP590 steel which shows martensite islands (dark phase) dispersed at the boundaries of the ferrite matrix (bright phase). The volume fraction of martensite was estimated to be ~ 25%, and the mean grain size of ferrite was ~ 5 μm.

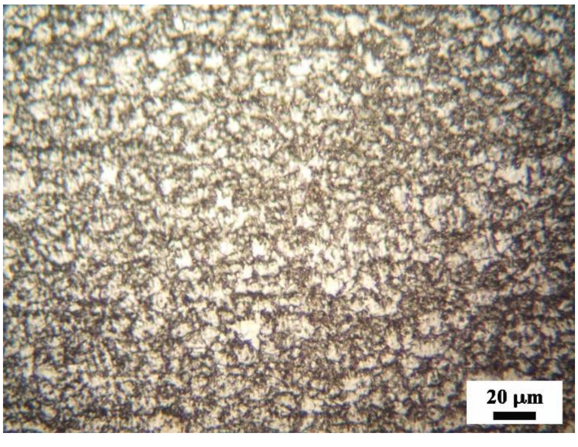

Fig. 3. OM image of the DP590 steel used in this study showing martensite islands (dark) in the ferrite matrix (bright).

OM images of typical microstructures of different areas across the LW400 sample is shown in Fig. 4. The microstructure of the FZ, as shown in Fig. 4a. was consisted entirely of lath martensite. This region experiences a high temperature above the melting point of steel. Consequently, grain growth is significant due to the elevated temperature, resulting in increased hardenability. Previous research has demonstrated that during LW of DP steels, the weld metal reaches peak temperatures as high as 2143 °C and subsequently solidifies at rapid cooling rates exceeding 10^4 °C/s [10]. Therefore, it is not surprising that martensite becomes the primary phase in the FZ. The microstructure in the CGHAZ (Fig. 4b.) was also consisted of lath martensite. Just outside the fusion boundary, the peak temperature is significantly higher than the critical temperature of A_3. As a result, there is significant growth of austenite grains, leading to high hardenability. Due to rapid cooling, the austenite transforms into lath martensite through shear phase transformation. The microstructure in the FGHAZ (Fig. 4c.) was composed of lath martensite and a small amount of grain boundary ferrite (white areas). The peak temperature in this zone is slightly above the critical temperature of A_3, limiting the growth of austenite grains and resulting in low hardenability. The relatively slow cooling rate causes austenite in this zone to transform into lath martensite and grain boundary ferrite. In the SCHAZ (Fig. 4d.), the microstructure was similar to that in the BM. The peak temperature in this area is below the critical temperature of A_1. Therefore, tempering of the pre-existing martensite is the main change in microstructure. The extent of tempering decreases as distance from the weld centerline increases.

Fig. 5. displays OM images of the microstructure of the FZ and CGHAZ for the LW450 and LW500 samples. In the FZ of the LW450 sample, grain boundary ferrite and Widmanstatten ferrite (WF) were observed besides martensite. Conversely, in the LW500 sample, the microstructure was primarily consisted of acicular ferrite (AF), WF, and martensite. Previous studies have shown that the cooling rate decreases with increasing the laser power or LW heat input [11]. This decrease in cooling rate promotes the formation of various types of ferrite alongside martensite. In the CGHAZ of the LW450 sample, the microstructure was almost fully martensitic. However, in the CGHAZ of LW500 sample, an amount of WF was also observed alongside martensite. The CGHAZ also revealed prior austenite grain boundaries as marked in Fig. 5b. and 5d. A comparison between the size of prior austenite grains in both samples showed that those in the LW500 sample were more than twice as large as those in the LW450 sample. This is due to lower heating and cooling rates in the latter, which allows for more grain growth in austenite. The lower cooling rate further encourages the formation of WF alongside martensite.

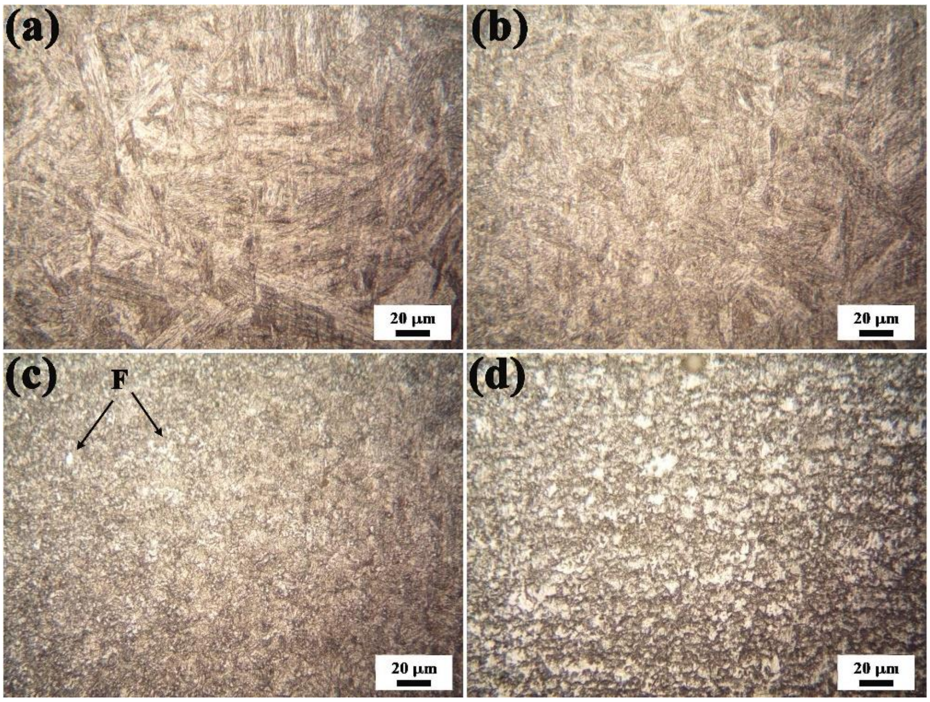

Fig. 4. OM images of different areas across the LW400 sample: (a) FZ, (b) CGHAZ, (c) FGHAZ, and (d) SCHAZ. F: ferrite

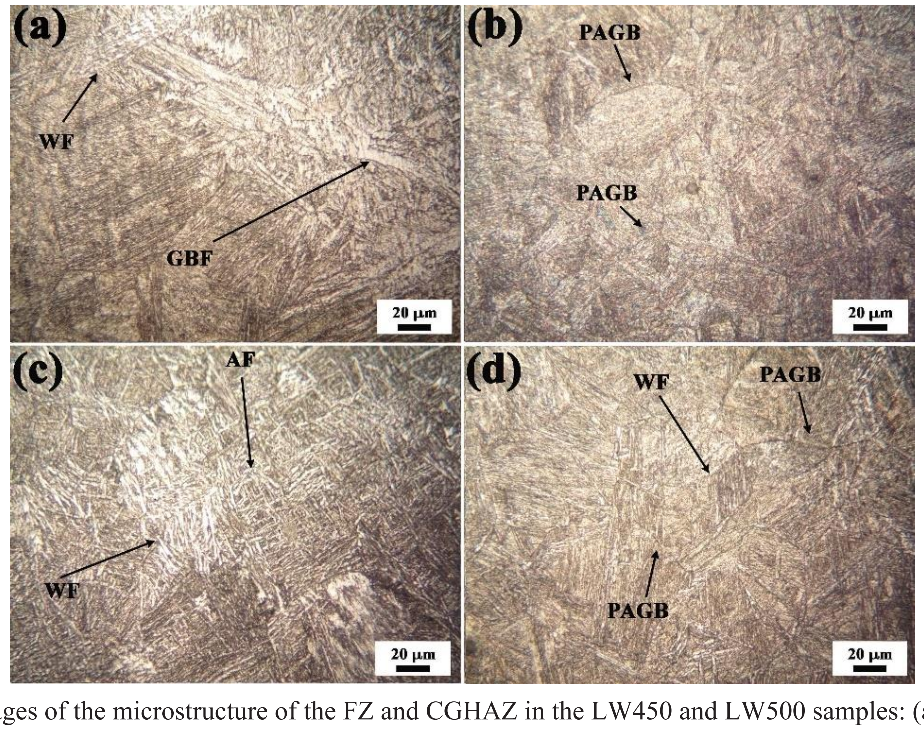

Fig. 5. OM images of the microstructure of the FZ and CGHAZ in the LW450 and LW500 samples: (a) FZ of LW450, (b) CGHAZ of LW450, (c) FZ of LW500, (d) CGHAZ of LW500. WF: Widmanestatten ferrite, GBF: grain boundary ferrite, PAGB: prior austenite grain boundary, AF: acicular ferrite.

3.2. Microhardness

Fig. 6. illustrates the microhardness profile of samples. The LW400 sample exhibited notably higher hardness values in the FZ and CGHAZ compared to the BM, with a mean hardness approximately twice of that the DP590 steel hardness. This increase can be attributed to the development of a fully martensitic microstructure, as shown in Fig. 4a. and 4b. In contrast, the LW450 and LW500 samples had lower hardness values in the FZ and CGHAZ

compared to LW400, but still higher than that of the BM. This decrease in hardness is due to the presence of ferrite alongside martensite, as shown in Fig. 5. In all samples, a decrease in hardness was observed in the HAZ, which is referred to as the softened zone [12]. The formation of this zone is primarily caused by partial tempering of the pre-existing martensite.

Variation of mean hardness value of FZ versus LW power is shown in Fig. 7a. It is observed that the hardness value of FZ linearly decreases with increasing the laser power. This can be attributed to the decrease in the cooling rate, which promotes the formation of ferrite instead of martensite. The percentage of softening (S) in the HAZ was also calculated and plotted versus the laser power in Fig. 7b. This parameter is defined as [13]:

$$S = \frac{H_{BM} - H_{Min}}{H_{BM}} \times 100 \qquad \text{Eq. (1)}$$

where H_{Min} is the minimum hardness in the HAZ and H_{BM} is the hardness of BM. As can be seen in Fig. 7b. the percentage of softening increases with increasing the laser power. However, the rate of increase in this parameter slowed down at higher laser power value. This is consistent with previous studies in the kinetics of softening in the HAZ of laser welded DP steels [8].

3.3. Tensile properties

Fig. 8. displays the stress-strain curves of both the BM and laser welded sheets at room temperature. A summary of the tensile properties is listed in Table 3. The DP590 steel flow curve exhibited typical characteristics of the tensile behavior of DP steels, such as continuous yielding behavior and a low YS to UTS ratio [14]. The LW400 sample failed in the FZ after a small amount of plastic deformation, resulting in a limited elongation in the stress-strain curve. However, for the other two welds, the YS was unaffected by welding and the UTS was only slightly reduced, leading to high joint efficiency values. Joint efficiency is defined as the ratio of the UTS of a welded sample to that of its respective BM [13]. Additionally, the total elongation of LW450 and LW500 samples was approximately half that of the DP590 steel. These two samples failed in the outer HAZ, which had the lowest hardness in the cross-section of the welds, as shown in Fig. 9.

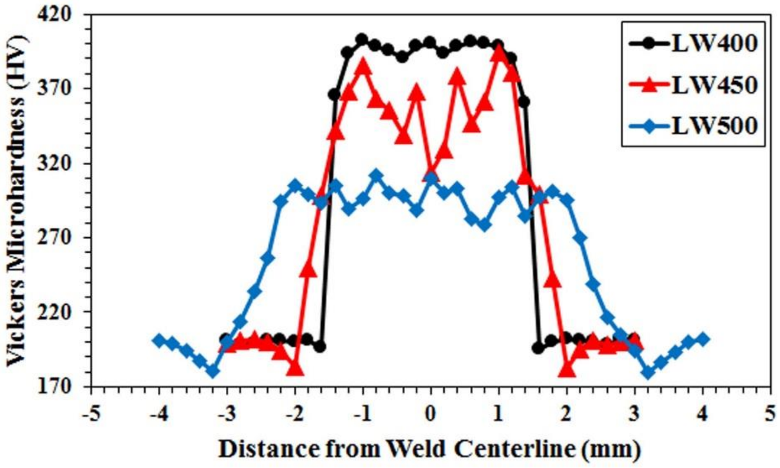

Fig. 6. Microhardness profile of different welds.

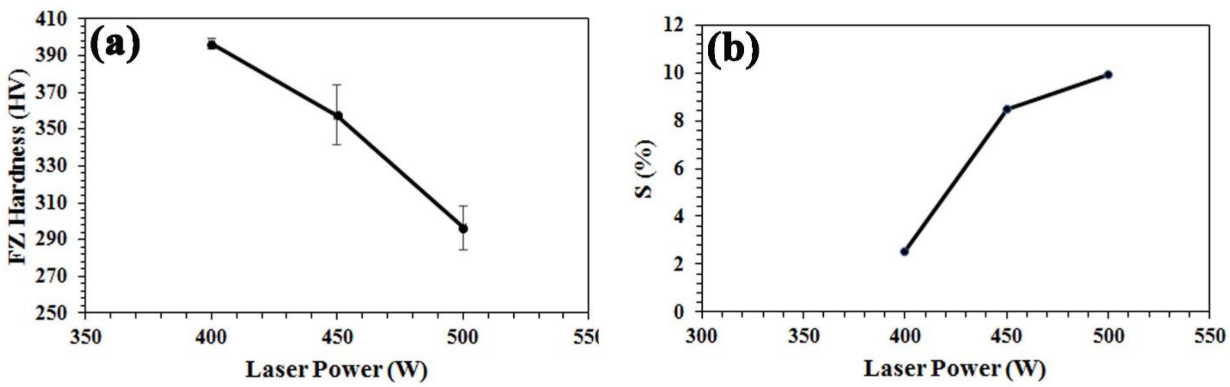

Fig. 7. (a) Mean hardness value of FZ versus the laser power, and (b) percentage of softening in the HAZ versus the laser power.

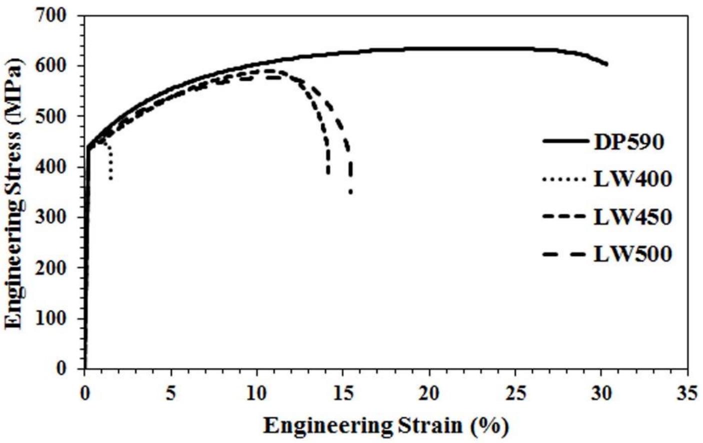

Fig. 8. Engineering stress-strain curves of the DP590 steel BM and welded samples.

Table 3. Summary of the tensile properties.

Sample	YS (MPa)	UTS (MPa)	TE (%)	JE (%)	Fracture location
DP590	437±1	638±2	29.1±0.2	-	-
LW400	439±1	452±3	1.5±0.3	70	Weld
LW450	435±3	590±2	14.1±0.2	92.5	HAZ
LW500	441±3	571±3	15.4±0.3	89.5	HAZ

Fig. 9. Failed samples of the welded joints.

3.4. Work hardening behavior

Based on the Kocks-Mecking approach [15], the work hardening behavior of different samples were analyzed by plotting the variation of the instantaneous work hardening rate (dσ/dε) against the true stress (σ), as shown in Fig. 10. All samples exhibited an initial rapid decrease in work hardening rate with true stress, followed by a linear decrease. This initial rapid decrease is referred to as the transient stage (TS), while the linear decrease at higher stresses is known as stage III work hardening [16]. The two-stage work hardening behavior has been previously observed in DP steels, with the first stage involving plastic deformation of ferrite and the second stage resulting from co-deformation of ferrite and martensite along with cross-slip of dislocations and dynamic recovery of ferrite [7]. A Comparison between the work hardening curve of the DP590 steel with that of laser welded joints demonstrated that the TS for the welded samples decreases at a faster rate compared to DP590 steel. This can be attributed to the tempering of martensite in the welded samples, as it was demonstrated that tempering of martensite in DP steels reduces the strain partitioning between the ferrite and martensite [17].

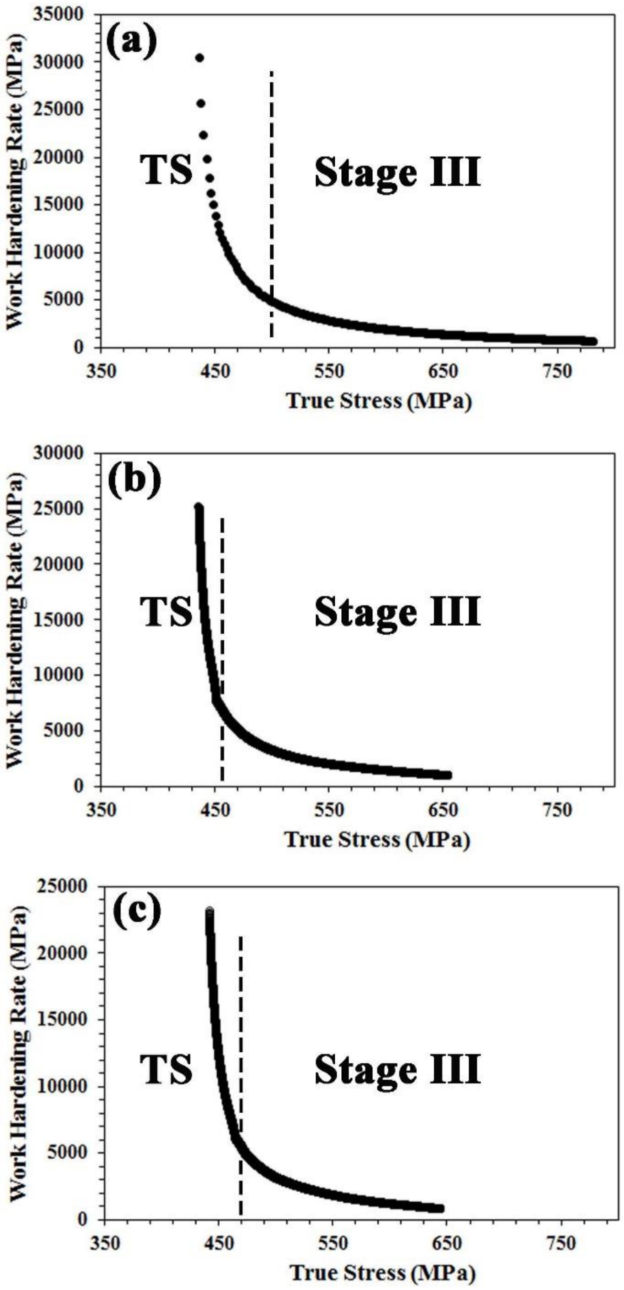

Fig. 10. Variations of instantaneous work hardening rate vs. the true strain for different samples. TS: transient stage.

The true stress- true strain relation in the uniform deformation stage can be expressed by the Hollomon equation [18]:

$$\sigma = k\,\varepsilon^{n} \qquad \text{Eq. (2)}$$

where σ is the true stress, ε is the true strain, n is the work hardening exponent and k is the strength constant. The work hardening exponent is directly related to the formability of material. Its higher value indicates higher deformability before instability [19]. In this case, the values of n for the DP590 steel BM, LW450, and LW500 samples were found to be 0.18, 0.15, and 0.14 respectively. These values suggest that the formability of the DP590 steel sheet decreases after LW process.

4. Conclusions

In this study, the effect of laser power on microstructure and tensile properties of laser welded DP590 steel sheet was studied and the following conclusions was derived:

- The microstructure of the FZ in the sample welded using a laser power of 400 W was consisted entirely of martensite. However, in the joints created using laser powers of 450 and 500 W, both WF and AF were also present alongside martensite. The presence of martensite in the FZ of the welded samples resulted in a significant hardness increase.
- The HAZ of all welds showed a region where the hardness decreased below that of the base metal due to the partial tempering of the pre-existing martensite. The degree of softening increased as the laser power was raised.
- The sample welded with laser power of 400 W failed in early stages of tensile test due to the lack of penetration defect. However, joints prepared with laser powers of 450 and 500W both failed in the softened zone, and exhibited YS values similar to the BM and joint efficiencies of 92.5% and 89.5%, with a significant reduction in elongation.
- The DP590 steel and welded joints showed a two-stage work hardening behavior corresponding to a TS followed by stage III hardening. Compared with the DP590 steel, the TS in the welded joints showed a higher decreasing slope.

References

[1] Mansur V.M, Mansur R.A.d.F, Carvalho S.M.d, Siqueira R.H.M.d, Lima M.S.F.d, Effect of laser welding on microstructure and mechanical behaviour of dual phase 600 steel sheets, Heliyon. 2021; 7: e08601.

[2] Ashrafi H, Shamanian M, Emadi R, Saeidi N, A novel and simple technique for development of dual phase steels with excellent ductility, Mater Sci Eng A. 2017; 680: 197-202.

[3] Ashrafi H, Shamanian M, Emadi R, Sarmadi M.A, Dual phase steel welded using friction stir welding and gas tungsten arc welding, steel research int. 2018; 89: 1700427.

[4] Wang J, Li W, Zhu X, Zhang L, Effect of martensite morphology and volume fraction on the low-temperature impact toughness of dual-phase steels, Mater Sci Eng A. 2022; 832: 142424.

[5] Ashrafi H, Shamanian M, Emadi R, Sanayei M. Farhadi F. Szpunar J.A. Characterization of microstructure and microtexture in a cold-rolled and intercritically annealed dual-phase steel, J Mater Eng Perform. 2021; 30: 7306-13.

[6] Dong D, Liu Y, Yang Y, Li J, Ma M.Jiang T, Microstructure and dynamic tensile behavior of DP600 dual phase steel joint by laser welding, Mater Sci Eng A. 2014; 594: 17-25.

[7] Farabi N, Chen D.L, Zhou Y, Microstructure and mechanical properties of laser welded dissimilar DP600/ DP980 dual-phase steel joints, J Alloy Cmpd. 2011; 509: 982–9.

[8] Xia M, Biro E, Tian Z, Zhou Y.N, Effects of heat input and martensite on HAZ softening in laser welding of dual phase steels, ISIJ Int. 2008; 48: 809-14.

[9] Mostaan H, Saeedpour P, Ahmadi H, Nouri A, Laser welding of dual-phase steels with different silicon contents: Phase evolutions, microstructural observations, mechanical properties, and fracture behavior, Mater Sci Eng A. 2021; 811: 140974.

[10] Kundu J, Ray T, Kundu A, Shome M, Effect of the laser power on the mechanical performance of the laser spot welds in dual phase steels, J Mater Process Technol. 2019; 267: 114–23.

[11] Jia Q, Guo W, Li W, Peng P, Zhu Y, Zou G, et al. Experimental and numerical study on local mechanical properties and failure analysis of laser welded DP980 steels, Mater Sci Eng A. 2017; 680: 378-87.

[12] Wei C, Zhang J, Yang S, Tao W, Wu F, Xia W, Experiment-based regional characterization of HAZ mechanical properties for laser welding, Int J Adv Manuf Technol. 2015; 78: 1629–40.

[13] Ashrafi H, Shamanian M, Emadi R, Sarmadi M.A, Effect of welding parameters on the microstructure and tensile properties of friction stir-welded DP600 steel, SAE Int J Mater Manuf. 2019; 12: 165-77.

[14] Ashrafi H, Shamanian M, Emadi R, Saeidi N, Correlation of tensile properties and strain hardening behavior with martensite volume fraction in dual-phase steels, Trans Indian Inst Met. 2017; 70: 1575–84.

[15] Kocks U.F, Mecking H, Physics and phenomenology of strain hardening: the FCC case, Prog Mater Sci. 2003; 48: 171-273.

[16] Mecking H, Kocks U.F, Kinetics of flow and strain-hardening, Acta Metall. 1981; 29: 1865-75.

[17] Ashrafi H, Shamanian M, Emadi R, Aghili S.E, Ghassemali E, Damage micromechanisms in friction stir-welded DP600 steel during uniaxial tensile deformation, J Mater Eng Perform. 2022; 31: 10044-53.

[18] Hollomon J.H, Tensile deformation, Am Inst Min Metall Eng Trans Iron Steel Div. 1945; 162: 268–89.

[19] Farabi N, Chen D.L, Zhou Y, Tensile properties and work hardening behavior of laser-welded dual-phase steel joints, J Mater Eng Perform. 2012; 21: 222-30.